This is an Accepted Manuscript for *Journal of Glaciology*. Subject to change during the editing and production process.
DOI: 10.1017/jog.2024.35

Topographic and hydrological controls on partial and full surges of Little Kluane Glacier, Yukon

Brittany Main[1,3], Luke Copland[1], Gwenn Flowers[2], Christine Dow[3], Wesley Van Wychen[3], Sergey Samsonov[4], Will Kochtitzky[5]

[1] University of Ottawa, Ottawa, Ontario, Canada
[2] Simon Fraser University, Vancouver, British Columbia, Canada
[3] University of Waterloo, Waterloo, Ontario, Canada
[4] Canada Centre for Mapping and Earth Observations, Ottawa, Ontario, Canada
[5] School of Marine and Environmental Programs, University of New England, Biddeford, ME, USA

ABSTRACT

We demonstrate that a ~20 km long valley glacier in the St. Elias Mountains, Yukon, can experience both partial and full surges, likely controlled by the presence of a topographic constriction and the formation and drainage of supraglacial lakes. Based on analysis of air photos, satellite images, and field observations since the 1940s, we identify a full surge of 'Little Kluane Glacier' from 2013 to 2018, and a partial surge of just the upper north arm between 1963 and 1972. Repeat digital elevation models (DEMs) and velocity profiles indicate that the recent surge initiated from the upper north arm in 2013, which developed into a full surge of the main trunk from 2017 to 18 with peak velocities of ~3600 m a^{-1} and frontal advance of ~1.7 km from May to September 2018. In 2016, a mass movement from the north arm to the main trunk generated a surface depression in a region immediately downstream of a topographic constriction, which promoted the formation and rapid drainage of supraglacial lakes to the glacier bed, and likely established the conditions to propel the initial partial surge into a full surge. Our results underscore the complex interplay between glacier geometry, surface hydrology and topography required to drive full surges of this glacier.

1. INTRODUCTION

Surge-type glaciers are typically characterized by short periods of rapid flow (active phase), interspersed with extended periods of slow or near-stagnant flow (quiescence) (e.g., Benn and Evans, 2010). During the quiescent phase, low ice velocities result in ice mass build up in the reservoir zone, often located in the glacier's accumulation area, while substantial mass is lost in the receiving zone down-glacier, usually located in the ablation area. When a surge occurs, ice mass is rapidly redistributed from the reservoir to the receiving zone, often resulting in thinning in the reservoir zone, thickening in the receiving zone, and an advance of the glacier front in some cases (e.g., Jiskoot, 2011; Benn and Evans, 2010). Surge-type glaciers comprise only ~1% of glaciers globally, and are primarily concentrated in specific regions including Alaska-Yukon, where at least 322 surge-type glaciers have been identified through direct observation of physical changes such as increased velocity and rapid terminus advance, or due to the occurrence of indicative features such as looped surface moraines (Post, 1969; Clarke and others, 1986; Clarke and Holdsworth, 2002; Sevestre and Benn, 2015).

Theories of surge initiation in temperate glaciers have focused on hydrologic triggers based on transformation of the subglacial drainage system from channelized to distributed (Kamb and others, 1985; Kamb, 1987; Fowler, 1987; Murray and others, 2003). While the duration of surge events and their recurrence interval are unique to each glacier, surges of temperate glaciers typically last for ~1-2 years, with an intervening quiescent phase of a decade or longer (e.g., Eisen and others, 2001, 2005; Bevington and Copland, 2014; Sevestre and Benn, 2015; Kochtitzky and others, 2019). However, growing evidence suggests that glacier flow instabilities exist with a spectrum of characteristics and on variable timescales, making a simple definition of surging challenging (e.g., Herreid and Truffer, 2016; Truffer and others, 2021). For example, the term "mini-surges" has been used to describe short-term velocity pulses over a period of hours, followed by a gradual decline in velocity throughout the following day, which occur prior to a glacier surge after the reservoir has refilled with sufficient mass (e.g., Variegated Glacier; Harrison and others, 1986; Kamb and Engelhardt, 1987). Sund and others (2009) also describe partial or "invisible" surges, whereby there is a major mass movement in an upper basin, which does not result in a surge of the main trunk of a glacier, and does not result in a terminus advance.

Recently, studies have attempted to reconcile existing surging theories into an over-arching enthalpy theory, which suggests that surging exists where enthalpy gains (e.g., from balance

https://doi.org/10.1017/jog.2024.35 Published online by Cambridge University Press

velocities) cannot be effectively balanced by enthalpy losses (e.g., from heat conduction and meltwater discharge) (Benn and others, 2019; Benn and others, 2023). However, there are still variations in surging behaviour that are not fully explained by this theory, and further observations and analyses are required to understand surging behaviour.

It is useful to investigate surge-type glaciers to advance our understanding of dynamic ice-flow instabilities, and to better disentangle glacier-climate responses from internal variability (e.g., Yde and Paasche, 2010; Flowers and others, 2011). Frequently, there are limited records which encompass the evolution of glacier surges over both quiescent and active phases. Partial surges are in particular poorly documented, and therefore this study expands our understanding of the spectrum of surging behaviours. Additionally, on a local scale, glacier surges can be hazardous to communities and infrastructure due to their rapid mass redistribution, increased calving, and potential for the formation of ice dams and associated downstream flooding (Harrison and others, 2015; Painter and others, 2023). For example, Kochtitzky and others (2020) report how repeated surges of Dań Zhùr (Donjek) Glacier, located ~30 km downstream of the terminus of Little Kluane Glacier, have blocked the Dań Zhùr River and led to the formation of several ice-dammed lakes and associated glacial lake outburst floods. While overall a limited impact, oral histories attest to glacier outburst floods having had fatal consequences for members of local indigenous communities in the past (Cruikshank, 2001, 2005).

Here we provide the first report of a 2013-18 surge of "Little Kluane Glacier", Yukon, to expand upon knowledge of glacier surges and other ice-flow instabilities in the St. Elias Mountains. We describe the surge from beginning to end to quantify the initiation location and subsequent progression, using a variety of datasets including digital elevation models (DEMs), temporally dense records of ice velocity, and observations of changes in surface characteristics and terminus location. These observations are placed in the context of the behaviour of Little Kluane Glacier since the late 1940s, including the likelihood of a previous partial surge.

2. STUDY AREA

Located on the eastern side of the St. Elias Mountains in the traditional territory of Kluane and White River First Nations (Fig. 1), Little Kluane Glacier (60°45'N, 139°08'W) is ~20 km long and up to ~1.5 km wide, and ranges in surface elevation from ~1400 to 3500 m a.s.l. (Morin and

https://doi.org/10.1017/jog.2024.35 Published online by Cambridge University Press

others, 2023). The glacier was previously classified as a tributary of Kluane Glacier in the Randolph Glacier Inventory (RGI 6.0) (RGI Consortium, 2017), but from recent satellite imagery and historical air photos it is clear that these glaciers have not been connected since at least 1963 (Post, 1963). No official name exists for the glacier, but historical air photo surveys completed by Austin Post in 1963 and 1965 identified it as Little Kluane Glacier, so we use that name here.

Little Kluane Glacier is land-terminating, with a section of dead ice in front of the terminus. There are extensive looped moraines on the glacier surface, in particular on the northern side of the main trunk in the ablation area. There is limited debris cover on the glacier outside of the dead ice zone and moraines. In historical air photos, and until the 1990s, a northern tributary was connected to Little Kluane Glacier (Fig. 1), but since the early 2000s it has retreated significantly. The uppermost section of the glacier is divided into three main arms (here referred to as north, upper and south), all of which have several smaller cirque tributaries (Fig. 1). The upper and south arms converge approximately 14 km from the terminus. Ice-penetrating radar measurements at the confluence of the north arm and main trunk in July 2021 show a maximum ice thickness of ~173 m (Fig. S1). While no direct meteorological measurements exist within the glacier catchment, the climate on the eastern side of the St. Elias Mountains is generally characterized as arctic and continental, with prevailing low winter temperatures (Newman and others, 2020), although since 1970 temperatures have increased at all elevations between 2000 and 6000 m a.s.l. (Williamson and others, 2020).

3. METHODS

3.1 Data sources

To capture long-term changes in glacier geometry and surface features, historical air photos (1947-77), and optical satellite images from Landsat, Sentinel-2, RapidEye and PlanetScope (1972-2022) were obtained (Tables S1 and S2). The Royal Canadian Air Force (RCAF) acquired nadir photos during reconnaissance flights in 1947, 1951, 1972, and 1977, with the originals held in the National Air Photo Library, Ottawa; copies for this study were obtained from the University of Ottawa Map Library (https://www.uottawa.ca/library/collections/find-format/geospatial-data-maps) and the Yukon's Department of Energy, Mines and Resources Library (https://yukon.ca/en/science-and-

https://doi.org/10.1017/jog.2024.35 Published online by Cambridge University Press

natural-resources/research-and-monitoring/find-yukon-maps-energy-mines-and-resources) in Whitehorse. In addition, Austin Post flew a number of air photo surveys that captured Little Kluane Glacier in 1963 and 1965; these oblique images were obtained from the University of Washington Special Collections (https://www.lib.washington.edu/specialcollections/).

Landsat imagery was obtained from the United States Geological Survey Earth Explorer (https://earthexplorer.usgs.gov/) and downloaded in Level 1 GeoTIFF format. Sentinel-2 imagery was obtained from the ESA Copernicus Open Access hub and downloaded in Level-1C format (https://scihub.copernicus.eu/dhus/#/home). Images were preferentially selected from summer months under cloud-free conditions, with Landsat 1-3 (60 m resolution) and Landsat 5 (30 m resolution) imagery obtained in approximately 5-year intervals from 1972 to 2000, although suitable imagery during this time is sparse. Through an Education and Research Agreement with Planet Labs, RapidEye imagery (5 m resolution) was acquired from 2012-19, along with PlanetScope Level 3B Analytic MS imagery (3 m resolution) for summer 2018 (Planet Team, 2017). Some of the Planet imagery required further georectification and were aligned with a Sentinel-2 base image acquired on August 30, 2021, using distinctive bedrock and topographic features as tie points.

Glacier surface elevation changes before, during, and after the 2013-18 surge were characterized using DEMs from a variety of sources. DEMs were generated from SETSM WorldView imagery and ASTER Level 1A reconstructed unprocessed instrument data using the MMASTER software package (Girod and others, 2017; Table S4). Co-registration to the ASTER GDEM version 3 was completed using overlapping bedrock elevations (Shean and others, 2016). The produced ASTER DEMs have a 10 m vertical and 2 m horizontal uncertainty (Girod and others, 2017). The SPOT DEM used in this study is 30 m resolution, and available in L1A Level (radiometric equalization, no geometric correction) from the SPOT World Heritage Data Search (https://regards.cnes.fr/user/swh/modules/60), and has an estimated uncertainty of 6 m (Korona and others, 2009). A 2 m-resolution DEM produced from WorldView stereo pairs was obtained from the University of Minnesota Polar Geospatial Center (PGC), and has 3 m vertical accuracy (Noh and Howat, 2015). All DEMs were further co-registered to each other using the method outlined by Nuth and Kääb (2011).

https://doi.org/10.1017/jog.2024.35 Published online by Cambridge University Press

Glacier velocities were used to characterize behaviour prior to and after the 2013-18 surge. NASA's Inter-Mission Time Series of Land Velocity and Elevation (ITS_LIVE) program provides surface velocity mosaics derived from Landsat 4, 5, 7 and 8 imagery 1985-2018, with a resolution of 240 m, created via the auto-RIFT feature tracking processing chain explained by Gardner and others (2019) (Table S6). Velocity magnitude in m a^{-1} was extracted along the centrelines of Little Kluane Glacier (Fig. 1). The ITS_LIVE velocity dataset provides the error product *v_error* (error in velocity magnitude in m a^{-1}). Errors associated with the ITS_LIVE dataset, including surface skipping and sensor biases, are presented in the *Regional Glacier and Ice Sheet Surface Velocities Known Issues* documentation (Gardner and others, 2019). To calculate errors, the error values within the modified Little Kluane Glacier RGI v6.0 outline were extracted and averaged to provide an overall value (Table S6). The ITS_LIVE point comparison tool (https://itslive-dashboard.labs.nsidc.org/) was used to download velocities at specific locations along the glacier's surface (Fig. 1). The separation time was limited to between 0 and 200 days to focus on short-term velocity peaks. Winter (January-May) RADARSAT-2 ultra-fine image pairs were acquired by Parks Canada to generate surface velocity maps (Table S5). The majority of the image pairs have 24-day separation (RADARSAT-2 repeat orbit interval), although a few sets have 48-day separation due to acquisition conflicts.

Multiple field visits were made to Little Kluane Glacier between 2018 and 2022 to observe surface conditions and the evolution of the glacier during and after the 2013-18 surge. This included visual validation of the terminus and moraine positions identified in satellite imagery, ground-based surveys to measure ice thickness, and visual observations of the changes in crevassing, supraglacial hydrology and surface elevation over time. Ice thicknesses along a transect (Fig. 1, pink triangle) were obtained in a ground-based common-offset radar survey on 18 July 2021, using an IceRadar impulse radar system from Blue System Integration (BSI) Ltd. Due to heavy crevassing caused by the 2013-18 surge, the survey was limited to ~263 m. The original system described by Mingo and Flowers (2010) has been updated and used in multiple studies across the region (e.g., Wilson and others, 2013; Bigelow and others, 2020; Morin and others, 2023; Sharp and others, in revision). The transmitter pulse amplitude is ± 650V with a 2 ns rise time and pulse repeat frequency of 512 Hz. Transmitter and receiver were connected to resistively-loaded dipole antennas of 5 MHz centre frequency in ice. A time window of 8000 ns was used, corresponding to an ice depth of ~670 m, more than three times the maximum ice thickness along

https://doi.org/10.1017/jog.2024.35 Published online by Cambridge University Press

the transect. On-board stacking was used to reduce random noise while automatically sampling a full stack every 1-2 s. De-trending, low-pass filtering and gain control were applied before manually picking data with the BSI IceRadar Analyzer software. An assumed ice velocity of 1.68 $\times 10^8$ m s^{-1} was used to transform two-way travel time into ice depth (Bogorodskiĭ and others, 1985). Standard error analysis of this system suggests an ice thickness precision of ± 4 m, while an integrated single-frequency Garmin NMEA GPS18x has a reported horizontal accuracy of <3 m (Mingo and Flowers, 2010).

3.2 Terminus length and position

Terminus positions were mapped from 1947 to 2021 using a combination of historical air photos (1947-77) and optical satellite imagery (1972-2021) (Tables S1 and S2). These nadir photos were georectified to the same August 30, 2021, Sentinel-2 base image as was undertaken for the Planet imagery, using the same methodology. A minimum of 20 tie points were used to align each of the historical photos, although more were used if the image covered a larger area. Based on a comparison of fixed landmarks with cloud-free, snow-free Sentinel-2 imagery, the estimated georectification error averaged 13 m.

Terminus positions were traced manually, and the distance of the glacier terminus to a fixed reference line at the valley mouth close to Kluane Glacier was measured (Fig. 1). The maximum terminus extent was measured in each image, rather than an average across the glacier's width, as the terminus is narrow and typically well defined. However, there were limiting factors in the terminus position mapping, including the relatively low resolution of early imagery (1972-2000), shadowing from surrounding mountains, and extensive debris cover over the lowermost part of the glacier. To maintain consistency, the same person manually digitized all termini outlines, with uncertainties determined using the method described by Paul and others (2013). It is assumed that outline errors are equal to at least one pixel, resulting in a range in uncertainty from 3 – 60 m, with an average of 16.5 m as imagery is heavily skewed towards newer observations from higher resolution imagery.

https://doi.org/10.1017/jog.2024.35 Published online by Cambridge University Press

3.3 Supraglacial hydrology and surface features

The surface morphology of Little Kluane Glacier, including crevassing, supraglacial hydrology, and moraine positions, was characterized using the georectified nadir air photos and optical satellite imagery from 1951 to 2020 (Tables S1 and S2). These were used to identify and manually measure the length and area of temporally consistent supraglacial hydrologic features such as surface channels and lakes, and how supraglacial drainage patterns evolved before, during and after a surge. The supraglacial lakes were outlined in RapidEye imagery in 2016 using the same process as the terminus positions, and area uncertainty was assumed to be as high as 5%, ranging from 276 to 1628 m^2, as determined using the Paul and others (2013) method (Table S3).

The location and evolution of a series of looped moraines along the surface of Little Kluane Glacier were mapped in ~10-year intervals during quiescent periods, and as often as monthly during surge periods when suitable imagery was available. During quiescence, moraine positions were mapped from imagery taken between May and September, as snow often obscures the features at other times of the year. However, during surge periods it was possible to also map changes in moraines during the winter months. Changes in moraine position were quantified in relation to a set point up-glacier of the initial position of each moraine loop. Uncertainties in moraine locations are assumed to be within one pixel in the imagery used to map their position, following the methodology used for the terminus outlines (Paul and others, 2013), equating to 10 – 60 m for Landsat scenes (corresponding to the quiescent periods) and 3 – 10 m for Sentinel-2 and Planet imagery (coinciding with surge periods).

3.4 Digital Elevation Model (DEM) analysis

To compute surface elevation change between 2010 and 2019, the earliest SPOT DEM (03-09-2010) was subtracted from the most recent post-surge ASTER DEM (04-08-2019) to generate a DEM of Difference. As these DEMs have different sources, we co-registered them and compared their values over stable terrain to determine their uncertainty. Based on the largest uncertainty value of the two sources, this equated to an average of ± 10 m. Glacier surface elevation change was extracted at 10 m intervals along south and north arm centrelines (Fig. 1), and smoothed using a 300 m moving window to reduce noise. Mountains surrounding the glacier are steep, leading to data gaps and high comparative errors in these regions, although relative patterns on the glacier

https://doi.org/10.1017/jog.2024.35 Published online by Cambridge University Press

surface are clear. Changes in surface slope during the most recent surge were examined using a SPOT DEM (03-09-2010), and WorldView DEM (17-07-2016) (Table S4). Ice rim heights were estimated by extracting and analyzing elevation points from the 22-08-2020 ASTER DEM.

3.5 Winter velocity mapping

Knowledge of winter velocities was required as glacier surges often initiate in the late winter or early spring in the study region (Abe and Furuya, 2015). These were derived from SAR imagery as feature-tracking velocities computed from optical imagery, such as those provided through ITS_LIVE, are unreliable over short periods in the winter when visible features on the glacier surface are obscured by snow, shadow, and/or low light levels. SAR imagery also delivers accumulation-area velocities, which can be difficult to determine from optical imagery. Speckle-tracking was performed on winter (January-May) RADARSAT-2 ultra-fine image pairs to generate surface velocity maps (Table S5). GAMMA software was used to process the SAR image pairs, as it provides velocity results similar to other speckle-tracking methods previously applied in northern and western Canada (Waechter and others 2015; Van Wychen and others 2018). Based on co-registered backscatter intensity images, a patch intensity cross-correlation was used to determine displacement in the azimuth and range directions from the offset between corresponding pixel blocks in each image pair (Lu and Veci, 2016).

Velocities (in m a^{-1}) were filtered to remove noise and mismatches. Coarse filtering was used to retain values between 5 m a^{-1} and 5000 m a^{-1}, which represented the lower detection limit and maximum velocities previously measured in the St. Elias Mountains, respectively (Waechter and others, 2015). A custom Matlab script was used to automatically filter the data based on flow direction, where values that differed by >50° from the mean direction of neighbouring cells were discarded (Main and others, 2022). Where multiple image pair results from the same winter existed, overlapping values were averaged to produce a single velocity value, and Inverse Distance Weighted (IDW) interpolation was used to fill minor gaps (<250 m). The results were clipped to a modified Randolph Glacier Inventory version 6.0 outline, with Little Kluane Glacier separated from Kluane Glacier. Following a similar methodology to that used by Waechter and others (2015), velocities were extracted at 50 m horizontal intervals along centrelines (Fig. 1) and smoothed using a 100 m moving window.

https://doi.org/10.1017/jog.2024.35 Published online by Cambridge University Press

Variations in the satellite orbital model, poor image co-registration, DEM/cross-correlation errors, and layover or foreshortening effects in SAR imagery can create errors in speckle-tracking results (Schellenberger and others, 2016; Van Wychen and others, 2018). To quantify these errors, the apparent motion over stable ground was determined outside of a buffer of 100 m around the modified RGI v6.0 outline. The apparent motion is the average speed of all stable ground pixels, irrespective of x or y direction. We assume that this represents the uncertainty, with values ranging between 3 and 6 m a^{-1} for the 2014-20 RADARSAT-2 data (Table S5).

4. RESULTS

Results from this study are presented both chronologically and by dataset, from the earliest available results to the most recent.

4.1 Terminus position

The oldest available imagery of Little Kluane Glacier, a RCAF photo from 1947, indicates that the glacier terminus once pushed into Kluane Glacier, displacing the adjacent ice, and creating a slight bulge (Fig. 2a). This photograph only includes the lowermost section of the terminus of Little Kluane Glacier, with the bulge appearing to contain mainly dead ice as demonstrated by significant debris cover, potholes in the surface, and a lake and river near the valley mouth. This suggests that a surge of Little Kluane Glacier occurred some years before the image was acquired.

From 1947 to 1963 the terminus retreated by up to ~2000 m, but this was not constant across the terminus due to its irregular shape in 1947 (Fig. 2a). From 1963 to 1998 the terminus retreated gradually, with a total retreat of ~980 ± 60 m (~28 ± 1.7 m a^{-1}) (Figs. 2b and 2d). From 1998 until 2013, the rate of terminus retreat increased significantly, with a total loss of ~1650 ± 30 m (~110 ± 2 m a^{-1}). The terminus advanced by ~340 ± 15 m (~170 ± 7.5 m a^{-1}) between 2015 and mid-August 2017 then remained stable until the end of May 2018, when thickening at the terminus began. After this, the terminus advanced by an additional 1400 ± 15 m (~12 m d^{-1}), stagnating by September 2018 (Fig. 2c). Following surge termination in 2018 the terminus position was ~2900 ± 15 m short of its maximum position in 1947. From 2018 to 2022 the terminus remained mostly stagnant, with minor variations (within 70 m) and evidence of downwasting at

https://doi.org/10.1017/jog.2024.35 Published online by Cambridge University Press

the end of the terminus, although debris cover and shadowing made it difficult to detect small-scale changes.

4.2 Surface features

There were distinct changes in the crevassing and supraglacial hydrology of Little Kluane Glacier over the study period (Fig. S2). From 1977 until 2012 the surface was relatively smooth, with a ~1 km long supraglacial channel (Fig. S2) and small supraglacial lakes present on the surface of the north arm in the accumulation zone (Figs. 3a and 3b). This supraglacial channel remained in approximately the same position over several decades, as it was visible in the August 3 1977 air photo, as well as in later imagery up to 2013.

In 2013 crevasses were present over a small area of the upper north arm, as was the supraglacial channel (Fig. S2c). By 2015, significant crevassing had appeared (Fig. S2d) in an area where, in 2012, the surface was smooth (Fig. S2b). There was a progressive increase in the intensity of crevassing from 2015 to 2016 (Figs. S2d and S2e), and by mid-June 2016 the supraglacial channel had been interrupted near its head by new, larger crevasses. Extensive crevassing covered nearly the entire surface of the upper north arm (i.e., accumulation zone) to the connection with the main glacier trunk by June 2016. Crevassing in the south and upper arms was delayed by approximately a year compared to the north arm: in 2013-14 there was limited crevassing in the south and upper arms, followed by an increase in intensity from 2016-17, and finally a peak in crevassing intensity and extent by September 2018. Crevassing in the main glacier trunk began to increase in intensity between February and June 2018, was extensive by July 2018 (Fig. 3), and peaked in September 2018.

Starting in June 2016 two supraglacial lakes (Fig. 3) formed below the north arm-main trunk connection, in an area where no lakes were observed in prior imagery. The lakes reached a maximum size of ~17400 ± 860 m^2 on June 18, 2016, and ~32600 ± 1630 m^2 on June 29, 2016, and had almost completely drained by late July that year. Heavy cloud cover in May and June 2017 made it difficult to monitor the lakes during this period, and only the west lake was observed to redevelop. By July 2017, the glacier morphology had significantly changed, and the east lake did not develop. From mid-July until mid-August 2017 the west lake decreased in area, although due

https://doi.org/10.1017/jog.2024.35 Published online by Cambridge University Press

to its small size the uncertainty estimates are too high to produce reliable quantitative estimates of its area. By September 2017, the west lake had completely drained. In 2018 the lakes again formed in approximately the same positions, but were surrounded by significant crevassing and additional ice from the north arm (Fig. 3c). RapidEye imagery from July 27 to 28, 2018, show that the east lake drained entirely within a single day (Fig. 3b-c).

There were four teardrop-shaped moraines visible in the 1951 air photos, which can be interpreted as the product of past surges (Fig. 4a) (Meier and Post, 1969; Young and others, 2022): these features were located on the north side of the glacier, were relatively evenly spaced apart, and had similar structural appearances. Between 1972 and 1977, a new looped moraine (E) was created (Fig. 4b, 5). The oldest looped moraine, 'A', was visible in the record until 1994 (Fig. 4c), when it reached the terminus. The three moraine loops (C, D and E) moved a maximum of ~1 km over the 43-year period from 1972 to 2015 (Fig. 4e), with higher velocities up-glacier and an average of 25 m a^{-1}.

After 2015, a new moraine loop (F) was formed via the transfer of ice from the north arm to the main glacier trunk between October 2015 and February 2016 (Fig. 4d). Due to poor image quality during the winter it is difficult to pin-point exact timing, but movement of the new bulge (moraine F) continued until September 2016 (Fig. S3f), and then slowed for most of 2017 (Fig. S3g). The largest displacement occurred between November 2017 and June 2018 (Fig. S3h-k), slowing in August 2018 to background velocities through 2019 (Fig. S3j-l). Existing moraine loops C, D and E were each transported approximately 1.7 km down-glacier during this period (Fig. 4e). Loop B (the second oldest moraine visible beginning in 1951) was no longer visible on the glacier after 2019.

4.3 Surface elevation changes

Changes in the surface elevation of Little Kluane Glacier between 2001 and 2019 indicate a transfer of mass from the top of the north arm and the main glacier trunk (over an area of ~27.5 km^2) into the terminus region, resulting in an overall thickening of ~100 to 170 m ± 10 m in the lower 2.5 km of the glacier over an area of ~7.3 km^2 (Fig. 5). There was a corresponding thinning of up to ~90 m ± 10 m in the upper north arm basin (Fig. 5), which is evident from a stranded ice

https://doi.org/10.1017/jog.2024.35 Published online by Cambridge University Press

rim that remained attached to valley walls (Fig. S4). In contrast, the upper arm and the uppermost region of the south arm (12-17.5 km up-glacier) remained relatively stable, with the main mass movement occurring from the main glacier trunk (~15-11 km from terminus) (Fig. 5b). Thinning of the south arm was more limited in area and intensity, with losses up to 70 m ± 10 m along the south arm centreline (Fig. 5b). There is also evidence of localized thickening where the valley narrows, such as at the confluence between the north arm and the main glacier trunk.

Between 2010 and 2016, there were localized changes to the glacier surface slope. Specifically, the slope in the confluence region of the north arm with the main trunk reversed between 2010 and 2016 (Fig. 6a). In 2010, the slope of line A-A' was 4.5%, and B-B' was 5.2%, while in 2016 the reversed slope section of the survey line (Figs. 6c and 6d) had a slope of -2.5% and -9.3%, respectively. The reverse slope created a ~0.13 km^2 basin.

4.4 Surface velocities

Annual average velocities obtained from the ITS_LIVE dataset (Fig. 7) revealed three main dynamic phases between 1985 and 2013. First, there was a higher velocity period from 1985 to 1996, where velocities in the main trunk ranged from ~40 to 70 m a^{-1}, with lower (<25 m a^{-1}) velocities in the north arm. This was followed by a lower velocity period from 1997 to 2012, when velocities across the glacier centreline averaged 10 m a^{-1}, and never exceeded 50 m a^{-1}. Finally, during the third period from 2013 to 2018 maximum annual velocities progressively increased, beginning at ~40 m a^{-1} in 2013, ~70 m a^{-1} in 2014, ~100 m a^{-1} in 2015, ~260 m a^{-1} in 2016, ~375 m a^{-1} in 2017, and finally ~830 m a^{-1} in 2018 (Figs. 7 and S5). Velocities increased first in the north arm, followed by the main glacier trunk (Fig. S5a). Both the upper and south arms of the glacier retained relatively stable velocity patterns compared to the north arm and main trunk, with modest increases occurring mainly between 2016 and 2018.

Point measurements from ITS_LIVE image pairs (Fig. 1) indicate increasing velocities from 2016 through 2018 (Fig. S5). Mean velocity of points located in the north arm (Fig. S5a) showed steady increases through 2016, followed by slight decreases in 2017, before peaking in fall 2018. Velocities in the main trunk increased progressively towards the terminus, with a point ~12 km upglacier from the terminus (point 3) increasing in speed approximately one year prior to

https://doi.org/10.1017/jog.2024.35 Published online by Cambridge University Press

a point ~8 km upglacier from the terminus (point 2), and two years prior to a point ~4 km upglacier from the terminus (Point 1) (Fig. S5b). Mean velocities in the main trunk were steady from 2014-16 (<100 m a^{-1}), increased in 2017, and peaked at ~3600 m a^{-1} near the terminus in fall 2018 (Fig. S5b).

RADARSAT-2 wintertime velocities indicate increased ice motion along the north arm centreline from 2014 to 2020 (Fig. 8). In the upper accumulation zone of the north arm, velocities increased over 4 years, from 2014 to 2017 (Fig. 8b). In the main glacier trunk, velocities remained stable (~40 m a^{-1}) through 2014-15, then increased in 2016 and 2017, before decreasing to background levels in 2020 (Fig. 8a). The highest winter velocities (~1000 m a^{-1}) were recorded ~5 km up-glacier from the terminus in early 2018 (Fig. 8a).

5. DISCUSSION

Our observations indicate that Little Kluane Glacier underwent a full surge over the period 2013-18, with substantial changes in terminus position, supraglacial hydrology, crevassing, surface elevation and ice velocities. This is the only full surge to have occurred between 1947 and 2022. There is evidence that a partial surge occurred during the 1960s-70s, and that multiple surges occurred prior to 1947, although these are poorly constrained in terms of timing and velocities. We discuss the evidence for these events chronologically below.

5.1 Pre-1947 surges

The presence of large, looped moraines on the glacier surface suggest that at least four surges occurred prior to 1947. The spacing between each looped moraine increases from the terminus through the main trunk, from ~1100 m between loops B and C, to ~2500 m between loops D and E in 2013, which may reflect a more compressive flow regime toward the terminus, or increasing time between surging intervals. The distance between the moraines has remained mostly consistent since 1972, with only a slight decrease in distance (~200 m) between moraines closer to the terminus. Observations from the 1960-70's partial surge (section 5.2) and 2013-18 full surge (section 5.3) indicate that these looped moraines form from the episodic movement of mass from

https://doi.org/10.1017/jog.2024.35 Published online by Cambridge University Press

the north arm into a slower moving main glacier trunk (Fig. S3). A similar but increasing distance occurs between each loop, suggesting regularly occurring surges, although the timing between them is not well constrained. From 1989 to 2010, moraine loop B flowed down-glacier at an average rate of ~35 m a^{-1}, loop C at ~15 m a^{-1}, and loop D at ~25 m a^{-1}. If we take the average of this motion of 25 m a^{-1}, and use a contemporary glacier length of 17 km, this means that at least 4 partial or full surges must have occurred in the ~70 years prior to 1947 to produce them, assuming that mass balance and velocity conditions have remained relatively constant. When compared with only one observed partial surge and one full surge from 1947 to 2020, This implies that Little Kluane Glacier has experienced a decline in surging frequency, likely indicative of a slower filling of the reservoir zone and higher snowlines. This trend aligns with the prevailing strongly negative mass balance observed in the St. Elias Mountains (Hugonnet and others, 2021).

Studies from other glaciers have shown that potholes begin to form on the ice surface as early as four years after surge termination (Sturm, 1987; Partington, 2023). If we assume that the last full surge prior to 1947 behaved similarly to the 2013-18 full surge, then by comparing the development of the surge bulge with the well-developed pothole and surface channels covering the dead ice zone at the glacier terminus in 1947 (Fig. 2a), we suggest that the pre-1947 surge likely occurred within the prior decade. This means that there was a period of at least 70 years between the two most recent full surges. In Figure 2a, the terminus extends ~2.5 km further than the most recent advance; this might have been caused by a greater pre-surge extent, a larger pre-1947 surge, or a combination of both scenarios.

5.2 1960-70's partial surge of Little Kluane Glacier

Although no full surge occurred between 1947 and 2013, there is still evidence of dynamic variability during this time. Historical air photos demonstrate that the north arm pushed into the main trunk of Little Kluane Glacier between 1963 and 1972 (Fig. S3), although the terminus did not advance during this time, instead following the long-term pattern of >4 km retreat between 1947 and 2013 (Fig. 2d). This mass movement created moraine E (Fig. 4b, 5c), although it is smaller and more elongated compared to the other moraine loops, such as loop D.

https://doi.org/10.1017/jog.2024.35 Published online by Cambridge University Press

Partial surges are described by Sund and others (2009) as a phenomenon when a mass movement occurs but does not instigate a terminus advance. In terms of their proposed surge stages, this refers to when a surge does not develop past stage 2, where there is surface lowering in major parts of the reservoir zone and thickening in the receiving zone, but there is no pronounced acceleration across most of the glacier surface, nor is there a terminus advance. Sund and others (2009) hypothesize that surge-type glaciers may oscillate between weaker, partial surges and more developed, full surges, and that this behaviour may explain the long build-up phase of some glaciers. They argue that while small and partial mass movements from the reservoir zone may initially delay a full surge, they could also promote a large surge through the slower, more stable, and potentially enhanced buildup of ice mass.

Between 1963 and 1972, there was a mass movement originating from the north arm to the main trunk of Little Kluane Glacier that displaced the medial moraine by ~250 m (Fig. S3); however, this did not develop into a full surge by 1977, with the bulge remaining in essentially the same position and no evidence of glacier acceleration or terminus advance (Fig. S3d). Changes in glacier surface morphology, including curved or displaced medial moraines have been used to identify partial surges in Svalbard (Sund and others, 2009, 2014) and the Pamirs (Kotlyakov and others, 2008; Shangguan and others, 2016). We therefore interpret this as being a partial surge of Little Kluane Glacier. This event formed a new moraine loop (loop E, Fig. S3b-d).

5.3 Characteristics of the 2013-18 surge

The 2013-18 surge of Little Kluane Glacier was driven primarily by the transfer of a large mass of ice from the north arm that prompted a surge in the main trunk. The extensive photographic, velocity and elevation records for this glacier provide insights into surge-related processes, including the interplay between surface topography and hydrology. Increased velocities in 2013 provided the first signal of the impending surge, followed by intensifying crevassing through 2015 and 2016, which interrupted a prominent supraglacial channel near the head of the north arm (Fig. S2). As velocities and strain rates increase at the start of a surge, the larger stress results in intense crevassing, enhancing distributed water access to the glacier bed that may further increase velocities due to the reduction in basal friction, thereby establishing a positive feedback (Dunse and others, 2015; Gong and others, 2018). For Little Kluane Glacier, this increased crevassing

https://doi.org/10.1017/jog.2024.35 Published online by Cambridge University Press

appears to have caused the supraglacial hydrological network to change from a concentrated to a distributed system (Fig. S2), which over time may have influenced the englacial and subglacial hydrologic networks, as surface water was no longer entering the glacier interior and bed from a single point (Shepherd and others, 2009), but instead through multiple locations (Colgan and others, 2011). As there is a delay between the increased velocities beginning in 2013 and the mass movement in 2016, we hypothesize that the evolution of the surficial hydrological network resulted in an increasing volume of water at the glacier bed, thereby increasing basal sliding, and enhancing the movement of mass from the north arm to the main trunk of the glacier.

At Little Kluane Glacier, changes in surface slope and supraglacial hydrology at the junction between the north arm and main trunk may also play a role in defining whether a partial surge of the north arm develops into something closer to a glacier-wide surge. Glacier velocities in the main trunk began to increase noticeably in 2015, a year after velocities increased in the north arm (Figs. 7 and S5). Beginning in early winter 2016, movement of a large ice mass occurred from the north arm to the main trunk. The addition of this mass changed the surface topography of the main trunk above the confluence with the north arm, and created a reverse surface slope, allowing surface water to pool and form supraglacial lakes in 2016, which reformed and drained throughout 2017 and 2018 (Figs. 3, 6). The following winter (2018), the glacier entered the fast, active phase (Fig. S5b), first increasing in velocity near the confluence with the north arm (Fig. S5b, point 3), with the surge then propagating down-glacier. The formation and drainage of these lakes over several years, combined with incrementally increasing glacier velocities (~155 m a^{-2}) over a 3-year period suggest that there may have been a slow, and then rapid, shift between subglacial drainage configurations, whereby significant, localized water input to the bed over multiple seasons may have eventually overwhelmed the subglacial drainage network and provoked acceleration, until an efficient drainage network was able to form and evacuate the water (Kamb and others, 2015). Sund and others (2014) suggested that a tributary is able to initiate a surge in the main trunk only if the main trunk was already in stage 1 (initial surface lowering, increased velocities) or stage 2 (larger mass displacement down-glacier), and thus ready to reach the final surge stage. However, at Little Kluane Glacier, we hypothesize that the main trunk becomes topographically and hydrologically primed for the final surge stage over a period of several years prior to the secondary surge initiation. In the absence of subglacial hydrological observations, we cannot definitively show that the change in surface morphology or hydrology (e.g., formation of

https://doi.org/10.1017/jog.2024.35 Published online by Cambridge University Press

supraglacial lakes and water-filled crevasses) drove the main trunk into a surge, although this may be a process that could be observed during tributary-trunk surges on other glaciers (Bhambri and others, 2021).

In 2018 the surge front reached the glacier terminus region, and surface velocities peaked at ~1000 m a^{-1} during the winter (Fig. 8) and ~2200 m a^{-1} near the end of summer (Fig. S5b). The terminus began to advance in May 2018, which coincided with the highest recorded point velocity of ~3600 m a^{-1} approximately 4.5 km up-glacier from the terminus (Figs. 2, S5b). The terminus underwent a total advance of ~1.4 km over spring and summer 2018 (Fig. 2c), at a mean rate of 12 m d^{-1}. Similar to other glaciers in the region including Klutlan, Variegated and Bering (Altena and others, 2019; Jay-Allemand and others, 2011; Burgess and others, 2012), Little Kluane displayed a winter initiation, with the highest velocities occurring for a short period during the summer, and the surge terminated abruptly toward the end of the melt season. Considering the above characteristics, along with the already-discussed evidence of subglacial hydrological processes, we suggest that Little Kluane Glacier most closely resembles surges controlled by changes in basal water pressure, at least when considering the main trunk.

After the surge event, it is possible to classify zones of the glacier based on changes in surface elevation. The dividing threshold is a 0 ± 10m elevation change, which delineates the two zones as suggested by Pitte and others (2016). We therefore consider the region >10 km up-glacier from the terminus to be the reservoir zone (Fig. 5), and the zone from ~6 km to the terminus the receiving zone. The zone of minimal net surface elevation change, known as the dynamic balance line, occurs ~6 km up-glacier from the terminus. While the surge was mainly driven by ice movement from the north arm, ice mass from the south and upper arms was pulled along as the full surge developed in the main trunk, further suggesting that the main trunk was not in a surge phase prior to input from the north arm. The minor role of the south and upper arms in the surge is demonstrated by the relatively small changes in ice surface elevation above the south arm-main trunk confluence compared to the north arm basin (Fig. 5), and the minor change in ice surface elevation in the upper arm (Fig. 6a-b).

From the data presented above, we suggest that the surging behaviour of Little Kluane Glacier follows these main phases:

https://doi.org/10.1017/jog.2024.35 Published online by Cambridge University Press

1. Due to a constriction at the connection between the north arm and the main trunk (a narrow valley which is quite steep, with a trough at the bed (Fig. S1)), the glacier is unable to efficiently transfer mass from the north arm to the main trunk, resulting in mass accumulation within the basin during quiescence.
2. After decades of accumulation, the ice mass in the north arm becomes thick enough that glacier velocities increase. Velocities increase over a period of 2-3 years, and crevasses begin to appear, disrupting persistent supraglacial drainage channels and routing water to the glacier bed in a distributed fashion.
3. Eventually the north arm ice mass is able to overcome the resistive forces acting upon it from the valley walls, bed, and abutment with the main trunk, resulting in a large mass movement from the tributary to the main trunk. In one instance (~1963-72) this did not initiate a full surge (Fig. S3).
4. Instigation of a full surge of the glacier may be facilitated by mass transfer from the north arm altering the surface slope below the junction of the north arm and main trunk (Figs. 3, 4), as occurred around 2016 (Fig. 6). A surface slope reversal allows water to pool and then drain into the glacier, possibly overwhelming the subglacial drainage system of the main trunk and initiating a surge there.
5. The surge front then propagates down-glacier, causing the terminus to advance, and driving enhanced ice motion in the south and upper arms due to a combination of longitudinal coupling with faster-flowing downstream ice, a steepening in surface slope, and a reduction in backpressure where they meet the main trunk.
6. Active surging ends as ice mass reaches the lower part of the glacier, lowering the driving stress and reducing glacier velocities to ~10 m a^{-1}. For Little Kluane Glacier, this coincided with the end of the melt season in September 2018.
7. The quiescent stage begins, and ice mass starts accumulating again in the north arm and along the main glacier trunk above the dynamic balance line.

https://doi.org/10.1017/jog.2024.35 Published online by Cambridge University Press

5.4 Comparison of the 2013-18 surge of Little Kluane Glacier with other surges in the St. Elias Mountains

Surging glaciers can be difficult to characterize due to lack of high-frequency temporal data from surge initiation through termination, resulting in uncertainties concerning where surges initiate, how they progress, the length of active/quiescent cycles, and whether a surge bulge is present. In Alaska-Yukon region, 322 surge-type glaciers have been previously identified (Sevestre and Benn, 2015), with 151 in the St. Elias Mountains of Yukon alone (Clarke and others, 1986). When compared to surges of some of the other glaciers in the region with comprehensive records (Dań Zhùr, Sít' Kusá, Nàłùdäy, and Variegated), the 2013 to 2018 surge of Little Kluane Glacier has a longer quiescent phase (~45 years compared to ~5-20 years for the others), and a long initiation phase (~5 years of initiation then ~1 year of intense surging, compared to 1-2 years of total active surging for the others). Several glaciers to the southeast, however, have quiescent phases exceeding 30 years. The most recent surges of Dusty Glacier (~80 km away) and Tweedsmuir Glacier (~140 km away) were <3 years in duration and preceded by quiescent intervals of ~36 years (Young, 2023) and ~34 years (Sharp, 2021), respectively. Fisher Glacier (~110 km away) had a quiescent phase of ~40 years, and an active phase of ~2.5 years, with a slow multidecadal increase in velocity between the mid-1980s and 2013 (Partington, 2023). Several smaller polythermal glaciers in the region, including Trapridge Glacier (Clarke and Blake, 1991; Frappé and Clarke, 2007) and "South Glacier" (De Paoli and Flowers, 2009), formerly surged in a manner similar to the glaciers above with multidecadal quiescent intervals, but more recently underwent prolonged "slow surges" where the high velocities associated with typical surges failed to develop.

5.5 Impact of geometric restrictions on glacier surging

Other studies (Jiskoot, 2011; Abe and others, 2016; Kochtitzky and others, 2019; Nolan and others, 2021) have suggested that restriction of ice flow is crucial in influencing surging behaviour of specific glaciers. The restrictions affecting glaciers can take a number of forms, including bedrock sills and overdeepenings (Jiskoot, 2011; Flowers and others, 2011; Lovell and others, 2018), constrictions in valley width (Kochtitzky and others, 2019), trunk-tributary interactions (Kotlyakov and others, 2008; Sund and others, 2009; Jiskoot and others, 2017) and icefalls (Nolan and others, 2021). For some glaciers, these features may act as a potential barrier to efficient ice

https://doi.org/10.1017/jog.2024.35 Published online by Cambridge University Press

flow due to increased friction during quiescence, and hence may encourage mass (and thus, energy/enthalpy) to build up in the reservoir zone (Sevestre and Benn, 2015). For example, Eisen and others (2001) found that cumulative mass balance played a role in the duration of the surge cycle of temperate Variegated Glacier, which was influenced by the location of a bedrock sill.

At Little Kluane Glacier, we suggest that the narrow connection between the north arm and the main glacier trunk acts as a flow constriction that, along with the backstress of the much larger main trunk, restricts ice flow, allowing ice mass to build. Eventually, the ice mass accumulates sufficiently to steepen the surface slope and overcome the frictional forces at this constriction, inducing a mass movement. The size of this ice flux (either relatively small, as in 1960s-1970s, or large, as in 2013-18) results in either a partial or a full surge, which may be dependent on several factors, including the cumulative mass balance between surges, and/or the state of the subglacial hydrological network of the main trunk.

6. CONCLUSIONS

Little Kluane Glacier experienced a progressive increase in glacier velocities in the north arm basin from 2013 to 2017, prior to the initiation of a full surge which occurred in 2018. A total of six previous dynamic instabilities were identified based on the presence of looped moraines, which includes one full and one partial surge documented here. A partial surge was identified in the mid-1960s to early-1970s, whereby mass movement was observed from the north arm tributary to the main trunk, but did not initiate a full surge and was smaller than the mass displacements that occurred during the 2013-18 surge. It appears that the narrow connection between the north arm tributary and the main trunk is important in defining the nature and extent of surges through the creation of a flow restriction. Evidence for this is provided by the initiation of the 2013-18 surge at the very top of the tributary through increased crevassing, then a mass movement from the tributary to the main trunk 2 years later, followed by a full surge in the main trunk. Additional data are needed to determine whether topographic or geometric factors are underpinning glacier surges at other locations in the St. Elias Mountains, and therefore detailed valley and bed elevation profiles are necessary to fully understand the role that geometry plays in glacier surging in this region.

https://doi.org/10.1017/jog.2024.35 Published online by Cambridge University Press

This study demonstrates that unstable flow of Little Kluane Glacier depends on a number of factors which are not yet fully understood. These could include glacier geometry, whereby a partial surge may delay a full surge by dissipating a portion of the stored energy, and therefore appear to promote conditions that favour more gradual reservoir growth. Another hypothesis is that the initial mass movement from a tributary to the main glacier trunk could initiate a full surge by producing a reverse slope that establishes the necessary conditions for water to pool on the surface, which eventually drains and overwhelms the subglacial drainage network. This may act as the trigger that enables a partial surge to evolve into a full surge affecting most of the glacier area. This study underlines the importance of data frequency and resolution when describing dynamic instabilities, and highlights that there are a variety of intersecting behaviours that can occur during a surge.

7. DATA AVAILABILITY

The RADARSAT-2 glacier velocities generated for this study are available from the Polar Data Catalogue under CCIN reference number 13309. Original RADARSAT-2 data is available through MDA Geospatial Services (https://www.asc-csa.gc.ca/eng/satellites/radarsat2/order-contact.asp). All satellite imagery (Landsat, Sentinel-2, RapidEye, and Planet), air photos, and ITS_LIVE velocity products are publicly available from data sources listed in the methods.

8. AUTHOR CONTRIBUTIONS

BM and LC designed the study. BM processed the surficial hydrology, crevassing and moraine datasets, completed the analysis and wrote the initial draft of the manuscript with input from LC, GF, CD and WVW. GF, SS, and WK provided processed datasets. All authors revised the paper prior to submission.

https://doi.org/10.1017/jog.2024.35 Published online by Cambridge University Press

9. ACKNOWLEDGEMENTS

Fieldwork for this project was conducted on Kluane and White River First Nations Traditional Territory, and the authors thank the community and Parks Canada for permission to work there. Support for this research has been provided by the University of Ottawa Geographical, Statistical and Government Information library (particularly René Duplain, Pierre Leblanc and Hugo Crites), Canada Centre for Mapping and Earth Observation (Natural Resources Canada), Northern Scientific Training Program, Canadian Space Agency (RADARSAT Constellation Mission Data Utilization and Application Plan), Natural Sciences and Engineering Research Council of Canada, New Frontiers in Research Fund, Canada Foundation for Innovation, Canada Research Chairs Program, University of Ottawa Research Chairs Program, Ontario Research Fund, Parks Canada, Kluane Lake Research Station, Outpost Research Station, and Polar Continental Shelf Program. Support for travel to conferences and attendance of courses was generously provided by the ArcticNet Network of Centres of Excellence Canada Student Training Fund, GlacioEx, and RemoteEx. We thank Library and Archives Canada for providing the historical air photos. We are grateful for the thoughtful and constructive comments provided by editor R. Bhambri, and by three anonymous reviewers.

https://doi.org/10.1017/jog.2024.35 Published online by Cambridge University Press

10. REFERENCES

Abe T, Furuya M and Sakakibara D (2016) Brief communication: twelve-year cyclic surging episodes at Donjek Glacier in Yukon, Canada. *The Cryosphere* **10**(4), 1427-1432. doi: 10.5194/tc-10-1427-2016

Abe T and Furuya M (2015) Winter speed-up of quiescent surge-type glaciers in Yukon, Canada. *The Cryosphere*, **9**, 1183-1190. doi:10.5194/tc-9-1183-2015

Altena B, Scambos T, Fahnestock M and Kääb A (2019) Extracting recent short-term glacier velocity evolution over southern Alaska and the Yukon from a large collection of Landsat data. *The Cryosphere* **13**(3), 795-814. doi: 10.5194/tc-13-795-2019

Benn DI, and Evans DJA (2010) *Glaciers and Glaciation*, 2nd Edition. London, UK: Hodder Education, 789pp.

Benn DI, Fowler AC, Hewitt I and Sevestre H (2019) A general theory of glacier surges. *Journal of Glaciology* **65**(253), 701-716. doi: 10.1017/jog.2019.62

Benn DI, Hewitt IJ and Luckman AJ (2023) Enthalpy balance theory unifies diverse glacier surge behaviour. *Annals of Glaciology* **63**(87-89), 88-94. doi: 10.1017/aog.2023.23

Bevington A and Copland L (2014) Characteristics of the last five surges of Lowell Glacier, Yukon, Canada, since 1948. *Journal of Glaciology* **60**(219), 113-123. doi: 10.3189/2014JoG13J134

Bhambri R, Hewitt, K, Haritashya, UK, Chand, P, Kumar, A, Verma, A, Tiwari, SK and Rai, SK (2022) Characteristics of surge-type tributary glaciers, Karakoram. *Geomorphology*, **403**, p.108161. doi: 10.1016/j.geomorph.2022.108161

Bigelow DG, Flowers, GE, Schoof, CG, Mingo LD, Young EM and Connal BG (2020) The role of englacial hydrology in the filling and drainage of an ice-dammed lake, Kaskawulsh Glacier, Yukon, Canada. *Journal of Geophysical Research: Earth Surface*, **125**(2), e2019JF005110. doi: 10.1029/2019JF005110.

Bogorodskiĭ VV, Bentley CR and Gudmandsen PE (1985) Radioglaciology (Vol. 1). Springer Science & Business Media.

Burgess EW, Forster RR, Larsen CF and Braun M (2012) Surge dynamics on Bering Glacier, Alaska, in 2008-2011. *The Cryosphere* **6**, 1251-1262. doi: 10.5194/tc-6-1251-2012

Clarke GKC and Blake EW (1991) Geometric and thermal evolution of a surge-type glacier in its quiescent state: Trapridge Glacier, Yukon Territory, Canada, 1969–89. *Journal of Glaciology* **37** (125), 158–169. doi: 10.3189/S002214300004291X

Clarke GKC, Schmok JP, Ommanney SL and Collins SG (1986) Characteristics of surge-type glaciers. *Journal of Geophysical Research: Solid Earth* **91**(B7), 7165-7180. doi: 10.1029/JB091iB07p07165

Clarke GKC and Holdsworth G (2002) Glaciers of the St. Elias Mountains. In: Williams RS Jr. & Ferrigno JG (eds). *Satellite Image Atlas of Glaciers of the World* (pp. J301−J311). North America: U.S. Geological Survey Professional Paper 1386.

https://doi.org/10.1017/jog.2024.35 Published online by Cambridge University Press

Colgan W and 7 others (2011) An increase in crevasse extent, West Greenland: hydrologic implications. *The Cryosphere* **38**(18), L18502. doi: 10.1029/2011GL048491

Cruikshank J (2001) Glaciers and climate change: perspectives from oral tradition. *Arctic* **54**(4), 377-393. https://www.jstor.org/stable/40512394

Cruikshank, J (2005) *Do Glaciers Listen?: Local Knowledge, Colonial Encounters, and Social Imagination*. Vancouver, Canada: UBC Press. 288 pp.

De Paoli L and Flowers GE (2009) Dynamics of a small surge-type glacier using one-dimensional geophysical inversion. *Journal of Glaciology* **55**(194), 1101-1112. doi: 10.3189/002214309790794850

Dunse T, Schellenberger T, Hagen JO, Kääb A, Schuler TV and Reijmer CH (2015) Glacier-surge mechanisms promoted by a hydro-thermodynamic feedback to summer melt. *The Cryosphere* **9**, 197–215. doi: 10.5194/tc-9-197-2015

Eisen O, Harrison WD and Raymond CF (2001) The surges of Variegated Glacier, Alaska, U.S.A., and the connection to climate and mass balance. *Journal of Glaciology* **47**(158), 351-358. doi: 10.3189/172756505781829250

Flowers GE, Roux N, Pimentel S and Schoof CG (2011) Present dynamics and future prognosis of a slowly surging glacier. *The Cryosphere* **5**(1), 299-313. doi: 10.5194/tc-5-299-2011

Flowers G, Jarosch A, Belliveau P and Fuhrman L (2016) Short-term velocity variations and sliding sensitivity of a slowly surging glacier. *Annals of Glaciology* **57**(72), 71-83. doi:10.1017/aog.2016.7

Fowler AC (1987) A theory of glacier surges. *Journal of Geophysical Research: Solid Earth* **92**(B9), 9111-9120. doi: 10.1029/JB092iB09p09111

Frappé TP and Clarke GKC (2007) Slow surge of Trapridge Glacier, Yukon Territory, Canada. *Journal of Geophysical Research: Earth Surface* **112**(3), 1–17. doi: 10.1029/2006JF000607

Gardner AS, Fahnestock MA and Scambos TA (2019) [accessed Jan. 2022] ITS_LIVE Regional Glacier and Ice Sheet Surface Velocities. Data archived at National Snow and Ice Data Center; doi: 10.5067/6II6VW8LLWJ7.

Gardner AS, and others (2019) [accessed Jan. 2022] ITS_LIVE Regional Glacier and Ice Sheet Surface Velocities - Known Issues - Available at: http://its-live-data.jpl.nasa.gov.s3.amazonaws.com/documentation/ITS_LIVE-Regional-Glacier-and-Ice-Sheet-Surface-Velocities-Known-Issues.pdf

Girod L, Nuth C, Kääb A, McNabb R and Galland O (2017) MMASTER: Improved ASTER DEMs for Elevation Change Monitoring. *Remote Sensing* **9**(7), 704. doi: 10.3390/rs9070704

Gong, Y and 6 others (2018) Simulating the roles of crevasse routing of surface water and basal friction on the surge evolution of Basin 3, Austfonna ice cap. *The Cryosphere*, **12**, 1563-1577. https://doi.org/10.5194/tc-12-1563-2018

Harrison W, Raymond C and MacKeith P (1986) Short period motion events on Variegated Glacier as observed by automatic photography and seismic methods. *Annals of Glaciology* **8**, 82-89. doi: 10.3189/S0260305500001191

Harrison WD and 9 others (2015) Chapter 13: Glacier Surges. In Shroder JF, Haeberli W and Whiteman C (eds) Hazards and Disaster Series, Snow and Ice-Related Hazards, Risks and Disasters, Academic Press, 437-485. doi: 10.1016/B978-0-12-394849-6.00013-5

Herreid S and Truffer M (2016) Automated detection of unstable glacier flow and a spectrum of speedup behaviour in the Alaska Range. *Journal of Geophysical Research: Earth Surface* **121**(1), 64-81. doi: 10.1002/2015JF003502

Hugonnet, R, and 10 others (2021) Accelerated global glacier mass loss in the early twenty-first century. *Nature*, **592**, 726-731. doi: 10.1038/s41586-021-03436-z

Jay-Allemand M, Gillet-Chaulet F, Gagliardini O and Nodet M (2011) Investigating changes in basal conditions of Variegated Glacier prior to and during its 1982-1983 surge. *The Cryosphere* **5**(3), 659-672. doi: 10.5194/tc-5-659-2011

Jiskoot H. (2011) Glacier surging. In: Singh VP, Singh P and Haritashya UK (eds) *Encyclopedia of Snow, Ice and Glaciers*. Dordrecht, The Netherlands, Springer, 415-428.

Jiskoot H, Fox TA and Van Wychen W (2017) Flow and structure in a dendritic glacier with bedrock steps. *Journal of Glaciology* **63**(241), 912-928. doi: 10.1017/jog.2017.58Kamb B and 7 others (1985) Glacier surge mechanism: 1982–1983 surge of Variegated Glacier, Alaska. *Science* **227**(4686), 469–479. doi: 10.1126/science.227.4686.469

Kamb B (1987) Glacier surge mechanism based on linked cavity configuration of the basal water conduit system. *Journal of Geophysical Research: Solid Earth* **92**(B9), 9083–9100. doi: 10.1029/JB092iB09p09083

Kamb B and Engelhardt H (1987) Waves of accelerated motion in a glacier approaching surge: the mini-surges of Variegated Glacier, Alaska, U.S.A. *Journal of Glaciology* **33**(113), 27-46. doi:10.3189/S0022143000005311

Kochtitzky W and 6 others (2019) Terminus advance, kinematics, and mass redistribution during eight surges of Donjek Glacier, St. Elias Range, Canada, 1935 to 2016. *Journal of Glaciology* **65**(252), 565-579. doi: 10.1017/jog.2019.34

Kochtitzky W, Copland L, Painter M and Dow C (2020) Draining and filling of ice-dammed lakes at the terminus of surge-type Dań Zhùr (Donjek) Glacier, Yukon, Canada. *Canadian Journal of Earth Sciences* **57**(11), 1337-1348. doi: 10.1139/cjes-2019-0233

Korona J, Berthier E, Bernard M, Rémy F and Thouvenot E (2009) SPIRIT. SPOT 5 stereoscopic survey of polar ice: reference images and topographies during the fourth International Polar Year (2007–2009). *ISPRS Journal of Photogrammetry and Remote Sens*., **64**, 204–212. doi: 10.1016/j.isprsjprs.2008.10.005

Kotlyakov VM, Osipova GB and Tsvetkov DG (2008) Monitoring surging glaciers of the Pamirs, central Asia, from space. *Annals of Glaciology* **48**, 125-134. doi: 10.3189/172756408784700608

Lovell AM, Carr RJ and Stokes CR (2018) Topographic controls on the surging behaviour of Sabche Glacier, Nepal (1967 to 2017). *Remote Sensing of Environment* **210**, 434-443. doi: 10.1016/j.rse.2018.03.036

Lu J and Veci L (2016) Offset Tracking Tutorial: Sentinel-1 Toolbox. Array Systems Computing Inc.

Main B and 11 others (2022) Terminus change of Kaskawulsh Glacier, Yukon, under a warming climate: retreat, thinning, slowdown and modified proglacial lake geometry. *Journal of Glaciology* **69**(276), 936-952. doi: 10.1017/jog.2022.114

Meier MF and Post A (1969) What are glacier surges? *Canadian Journal of Earth Sciences* **6**(4), 807-817. doi: 10.1139/e69-081

Morin A, Flowers GE, Nolan A, Brinkerhoff D and Berthier E (2023) Exploiting high-slip flow regimes to improve inference of glacier bed topography. *Journal of Glaciology* **69**(275), 658-664. doi: 10.1017/jog.2022.121

Murray T, Strozzi T, Luckman A, Jiskoot H, and Chrisakos P (2003) Is there a single surge mechanism? Contrasts in dynamics between glacier surges in Svalbard and other regions. *Journal of Geophysical Research: Solid Earth* **108**(B5), 2237. doi:10.1029/2002JB001906

Newman AJ, Clark MP, Wood AW and Arnold JR (2020) Probabilistic spatial meteorological estimates for Alaska and the Yukon. *Journal of Geophysical Research: Atmospheres* **125**(22), e2020JD032696. doi: 10.1029/2020JD032696

Noh M and Howat I (2015) Automated stereo-photogrammetric DEM generation at high latitudes: surface extraction from TIN-based search minimization (SETSM) validation and demonstration over glaciated regions. *GIScience and Remote Sensing* **52**(2), 198-217. doi: 10.1080/15481603.2015.1008621

Nolan A, Kochtitzky W, Enderlin EM, McNabb R and Krutz KJ (2021) Kinematics of the exceptionally short surge cycles of Sít' Kusá (Turner Glacier), Alaska, from 1983 to 2013. *Journal of Glaciology* **67**(264), 744–758. doi: 10.1017/ jog.2021.29

Nuth C and Kääb A (2011) Co-registration and bias corrections of satellite elevation data sets for quantifying glacier thickness change. *The Cryosphere* **5**(1), 271-290. doi:10.5194/tc-5-271-2011

Painter M, Copland L, Dow C, Kochtitzky W and Medrzycka D (2023) Patterns and mechanisms of repeat drainages of glacier-dammed Dań Zhùr (Donjek) Lake, Yukon. *Arctic Science,* 1-13. doi: 10.1139/AS-2023-0001

Partington G (2023) Reconstructing the surge history and dynamics of Fisher Glacier, Yukon, 1948-2022. MSc thesis, University of Ottawa. doi: 10.20381/ruor-29290

Paul F and 19 others (2013) On the accuracy of glacier outlines derived from remote-sensing data. *Annals of Glaciology* **54**(63), 171-182. doi:10.3189/2013AoG63A296

Pitte, P, Berthier, E, Masiokas, MH, Cabot, V, Ruiz, L, Ferri Hidalgo, L, Gargantini, H and Zalazar, L. (2016) Geometric evolution of the Horcones Inferior Glacier (Mount Aconcagua, Central Andes) during the 2002–2006 surge. *Journal of Geophysical Research: Earth Surface*, **121**(1), pp.111-127. doi: 10.1002/2015JF003522

Planet Team (2017) Planet Application Program Interface: In Space for Life on Earth. San Francisco, CA. https://api.planet.com.

Post A (1969) Distribution of surging glaciers in western North America. *Journal of Glaciology* **8**(53), 229-240. doi: 10.3189/S0022143000031221

RGI Consortium (2017) Randolph Glacier Inventory – A Dataset of Global Glacier Outlines: Version 6.0: Technical Report, Global Land Ice Measurements from Space, Colorado, USA. Digital Media. doi: 10.7265/ N5-RGI-60

Schellenberger T, Van Wychen W, Copland L, Kääb A and Gray L (2016) An inter-comparison of techniques for determining velocities of maritime Arctic glaciers, Svalbard, using Radarsat-2 Wide Fine mode data. *Remote Sensing* **8**(9), 785. doi: 10.3390/rs8090785

Sevestre H and Benn D (2015) Climatic and geometric controls on the global distribution of surge-type glaciers: implications for a unifying model of surging. *Journal of Glaciology* **61**(288), 646-663. doi: 10.3189/2015JoG14J136

Shangguan D and 6 others (2016) Characterizing the May 2015 Karayaylak Glacier surge in eastern Pamir Plateau using remote sensing. *Journal of Glaciology* **62**(235), 944-953. doi: 10.1017/jog.2016.81

Sharp M (2021) Amplification of surface topography during surges of Tweedsmuir Glacier. MSc thesis, University of Calgary. doi: 10.11575/PRISM/39300

Shean DE and 6 others (2016) An automated, open-source pipeline for mass production of digital elevation models (DEMs) from very-high-resolution commercial stereo satellite imagery. ISPRS *Journal of Photogrammetry and Remote Sensing* **116**, 101–117. doi: 10.1016/j.isprsjprs.2016.03.012

Shepherd A, Hubbard A, Nienow P, King M, McMillan M and Joughin I (2009) Greenland Ice Sheet motion coupled with daily melting in late summer. *Geophysical Research Letters* **36**, L01501. doi:10.1029/2008GL035758

Sturm, M (1987) Observations on the distribution and characteristics of potholes on surging glaciers. *Journal of Geophysical Research: Solid Earth* **92**(B9), 9015-9022. doi: 10.1029/JB092iB09p09015

Sund M, Eiken T, Hagen JO and Kääb A (2009) Svalbard surge dynamics derived from geometric changes. *Annals of Glaciology* **50**(52), 50-60. doi: 10.3189/172756409789624265

Sund M, Lauknes TR and Eiken T (2014) Surge dynamics in the Nathorstbreen glacier system, Svalbard. *The Cryosphere* **8**, 623-638. doi: 10.5194/tc-8-623-2014

Truffer M and 10 others (2021) Chapter 13 - Glacier surges. In: Haeberli W and Whiteman C (eds.). *Snow and Ice-Related Hazards, Risks, and Disasters* (Second Edition), 417-466.

Van Wychen W, Copland L, Jiskoot H, Gray L, Sharp M and Burgess D (2018) Surface velocities of glaciers in western Canada from speckle-tracking of ALOS PALSAR and RADARSAT-2 data. *Canadian Journal of Remote Sensing* **44**(1), 57-66. doi: 10.1080/07038992.2018.1433529

Waechter A, Copland L and Herdes E (2015) Modern glacier velocities across the Icefield Ranges, St. Elias Mountains, and variability at selected glaciers from 1959 to 2012. *Journal of Glaciology* **61**(228), 624-634. doi: 10.3189/2015JoG14J147

Williamson SN and 9 others (2020) Evidence for elevation-dependent warming in the St. Elias Mountains, Yukon, Canada. *Journal of Climate* **33**, 3253–3269. doi: 10.1175/JCLI-D-19-0405

Yde JC and Paasche Ø (2010) Reconstructing climate change: Not all glaciers suitable. *Eos, Transactions American Geophysical Union* **91**(21), 189–90. doi: 10.1029/2010EO210001

Wilson NJ, Flowers GE and Mingo, L. (2013) Comparison of thermal structure and evolution between neighboring subarctic glaciers. *Journal of Geophysical Research: Earth Surface*, **118**(3), 1443-1459. doi: 10.1002/jgrf.20096

Young EM, Flowers GE, Jiskoot H, Gibson HD (2022) Kinematic evolution of kilometre-scale fold trains in surge-type glaciers explored with a numerical model. *Journal of Structural Geology* **161**(2022), 104644. doi: 10.1016/j.jsg.2022.104644

Young EM (2023) Reconstructing the mass balance, ice flow, and structural glaciology of a non-surge-type and surge-type glaciers in the continental St. Elias Mountains. PhD thesis, Simon Fraser University.

https://doi.org/10.1017/jog.2024.35 Published online by Cambridge University Press

LIST OF FIGURE CAPTIONS:

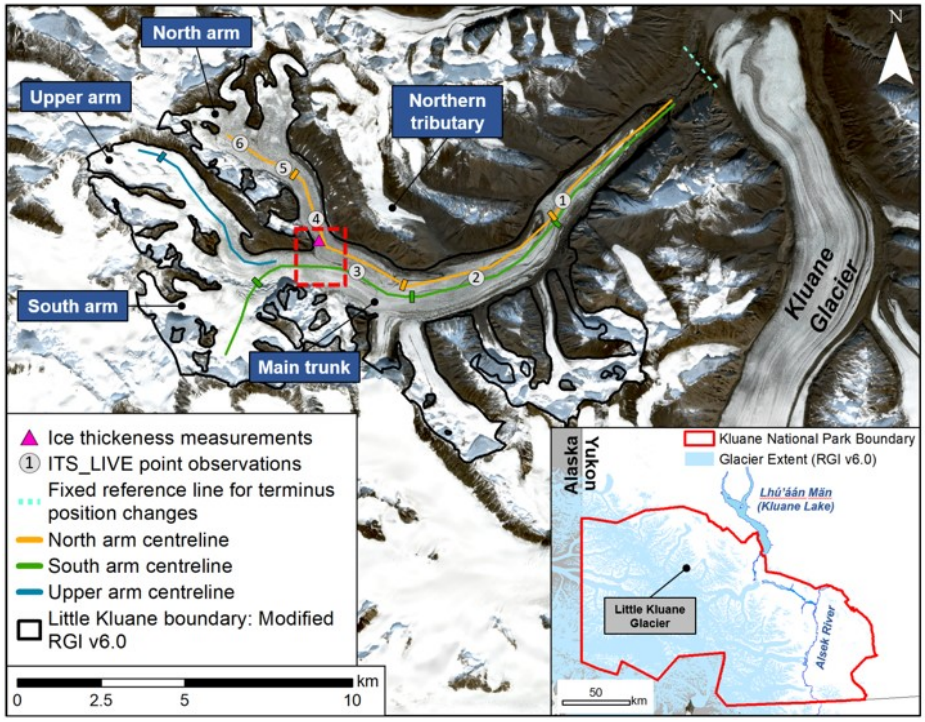

Figure 1: Little Kluane Glacier showing main locations referred to in the text. Red dashed box indicates region of interest in Figures 3 and 7. Note that the northern tributary disconnected from Little Kluane Glacier in the 1990s. The modified RGI outline is based on the glacier's post-surge position in 2019. Base image: Sentinel-2, 03-08-2019, UTM Zone 7N. Inset: Regional map of Kluane National Park and Reserve within the St Elias Mountains, with location of Little Kluane Glacier highlighted.

https://doi.org/10.1017/jog.2024.35 Published online by Cambridge University Press

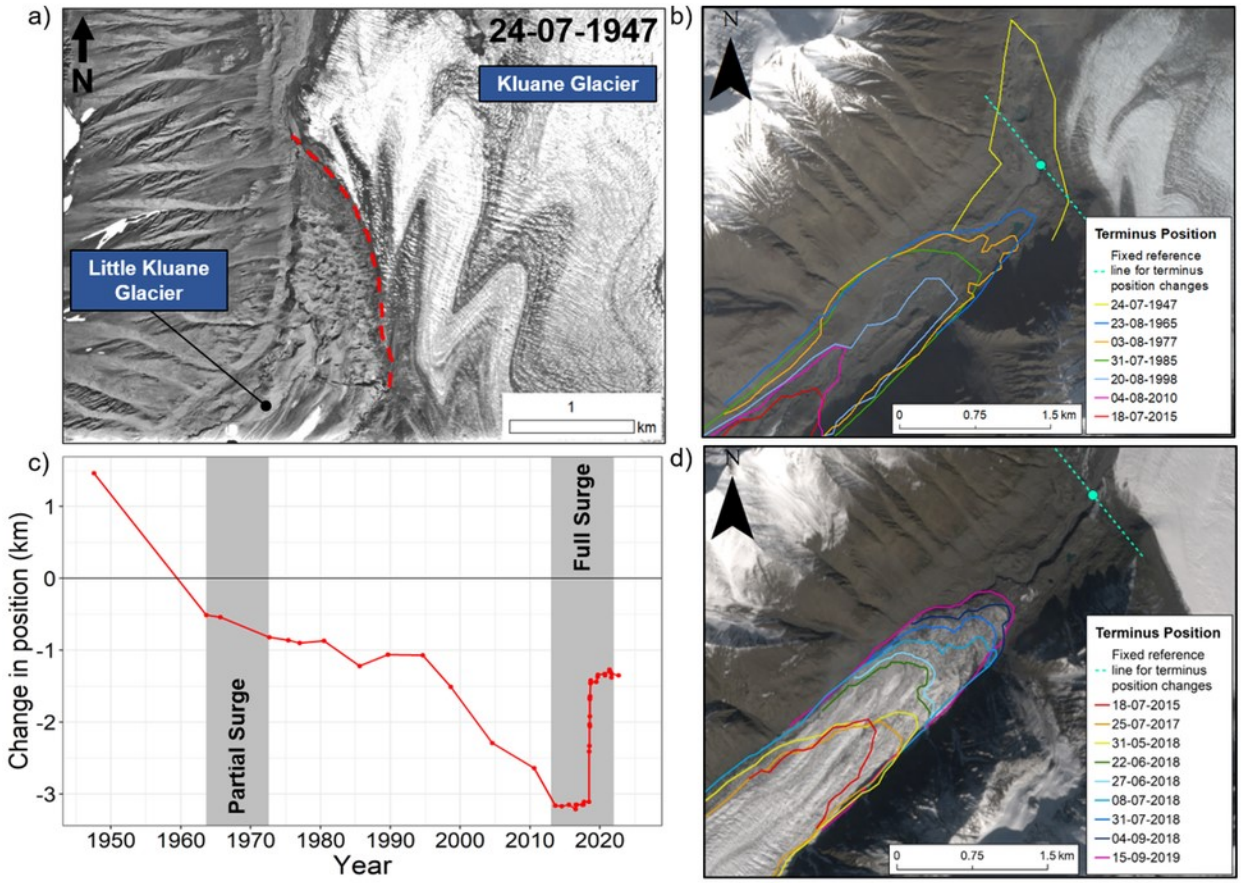

Figure 2: a) RCAF air photo from 24-07-1947, demonstrating how Little Kluane Glacier previously pushed into Kluane Glacier (image ID A11014-275). Red dashed line indicates the separation between Little Kluane and Kluane glaciers; b) Terminus positions of Little Kluane Glacier from 1947-2015. Projection: UTM 7N. Base image: Sentinel-2, 24-09-2016; c) Change in relative terminus position from 1947-2021 in relation to distance from valley mouth. Timing of partial surge (possible initiation range) and recent full surge are highlighted in grey; d) Terminus advance between 2015-2019, during recent surge. Base image: Sentinel-2, 30-08-2021.

https://doi.org/10.1017/jog.2024.35 Published online by Cambridge University Press

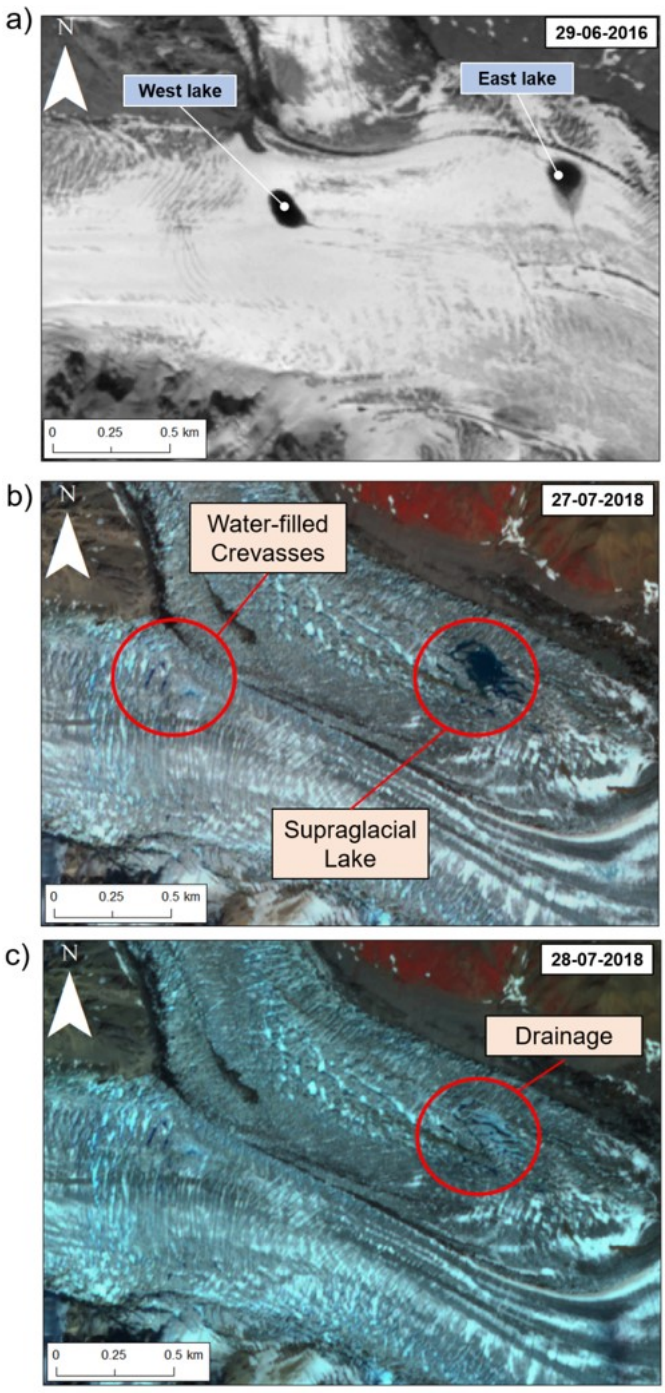

Figure 3: a) Supraglacial lake locations in 2016 (Fig. 7), on the surface of Little Kluane Glacier on 29-06-2016, during the active surge; b) Location of water-filled crevasses and supraglacial lake, on 27-07-2018; c) One day later on 28-07-2018, showing partial drainage of these features. Satellite images courtesy of Planet Labs. General location is indicated by red dashed box on Figure 1.

https://doi.org/10.1017/jog.2024.35 Published online by Cambridge University Press

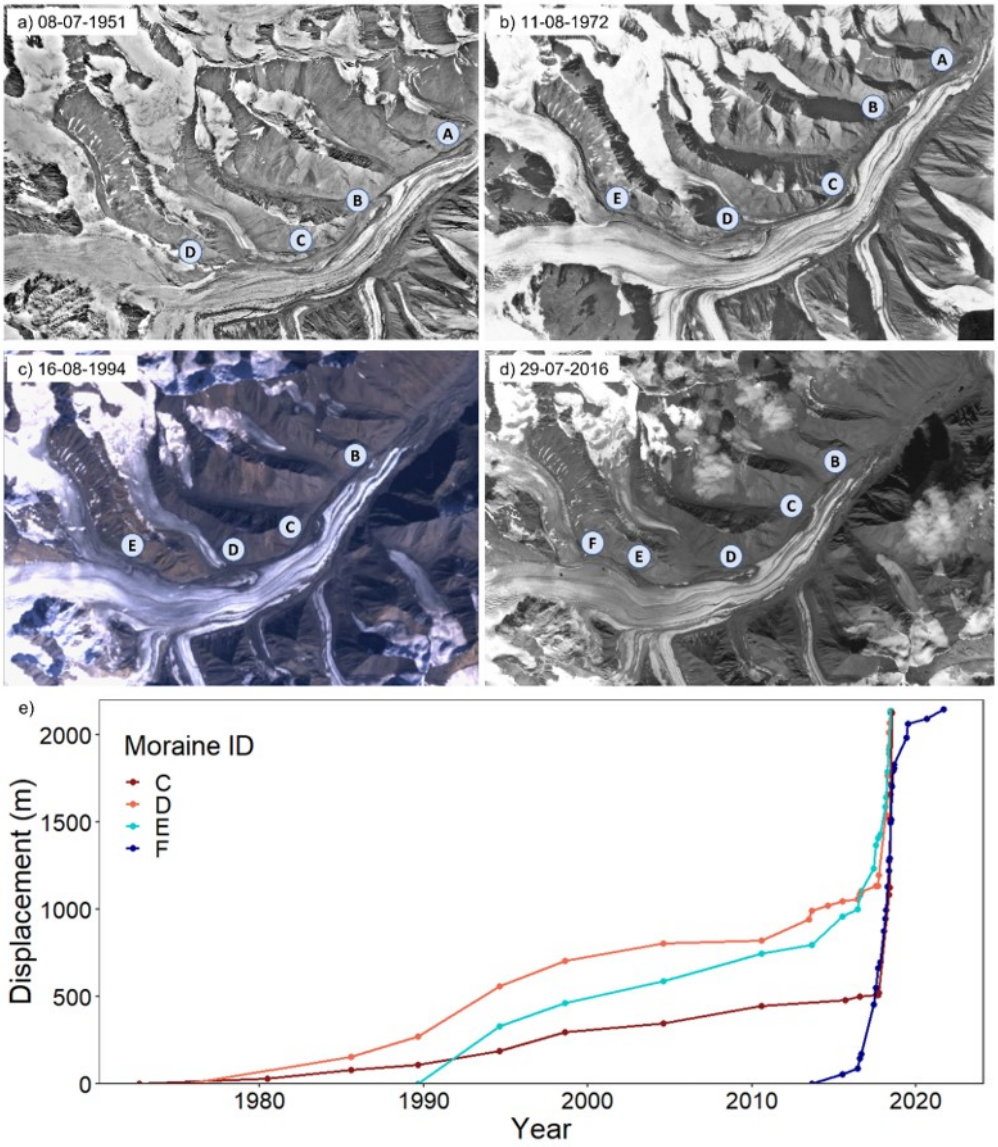

Figure 4: Looped moraine positions for each decade at Little Kluane Glacier in historical air photos (a-b) and satellite imagery (c-d) (listed in Table S1); a) 08 July, 1951; b) 11 August 1972; c) 16 August 1994; d) during surge initiation, 29 July 2016. Air photos are courtesy of the National Air Photo Library, Ottawa; e) Looped moraine movement from 1972-2021. Moraines A and B are not included as they disappear before the recent surge.

https://doi.org/10.1017/jog.2024.35 Published online by Cambridge University Press

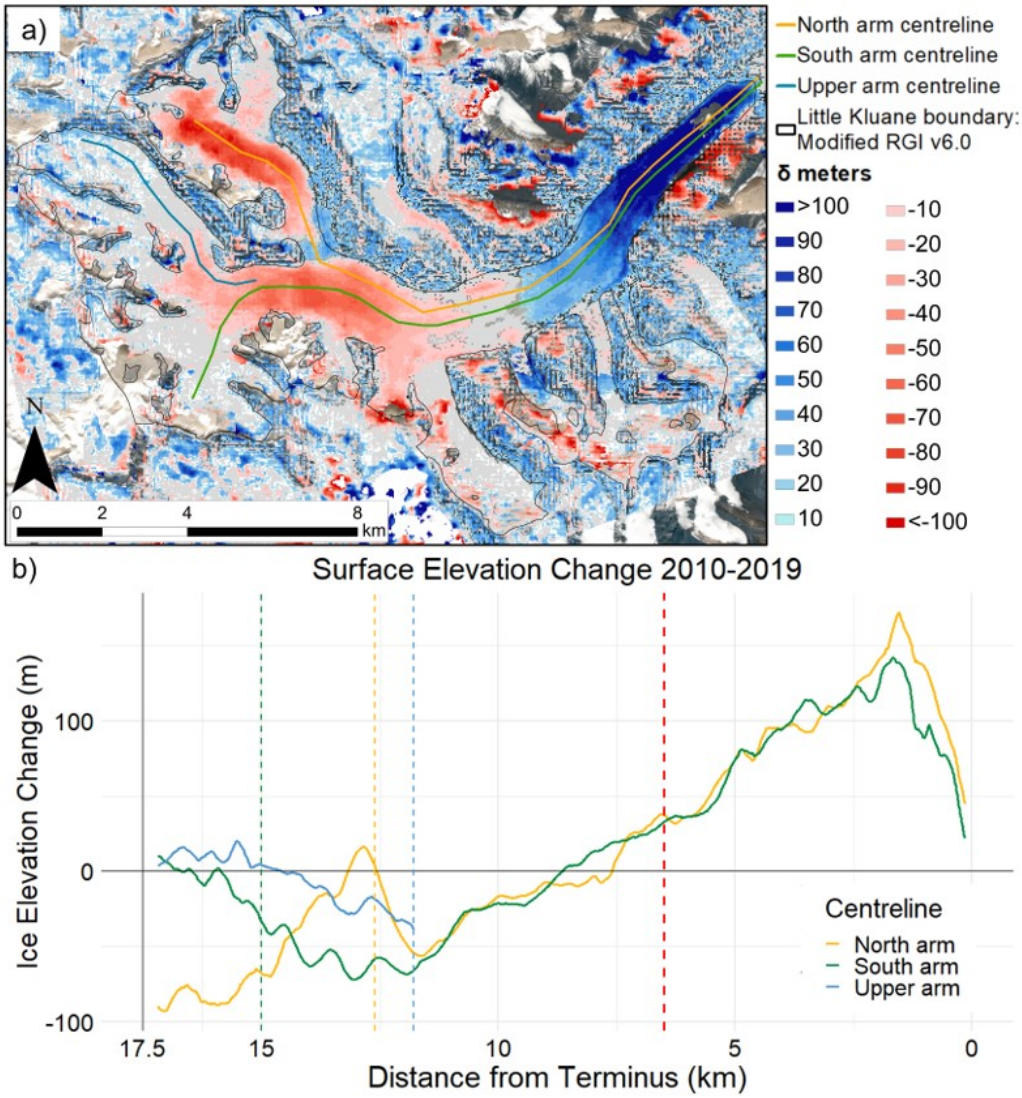

Figure 5: a) Elevation change across Little Kluane Glacier between 2010 and 2019, with overlain modified RGI 6.0 glacier outline and 2018 terminus extent. Projection: UTM 7N. Base image: Sentinel-2, 3 August, 2019; b) Little Kluane surface elevation change derived from a DEM of Difference between 2010 and 2019; dashed blue, green and yellow lines indicate where the respective arm connects to the main glacier trunk. Dashed red line indicates the location of the Dynamic Balance Line (DBL).

https://doi.org/10.1017/jog.2024.35 Published online by Cambridge University Press

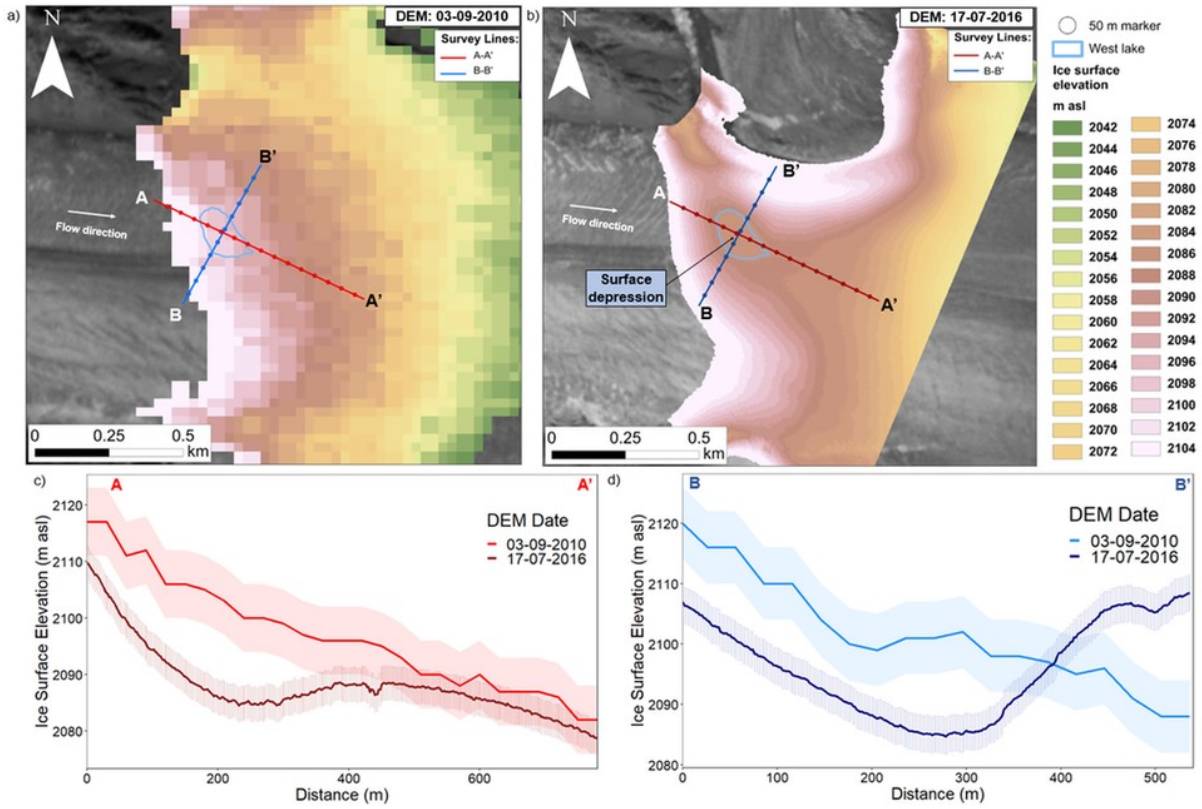

Figure 6: Changes in glacier surface topography after surge initiation. General location is indicated by red dashed box on Figure 1. a) SPOT DEM of glacier surface on 03-09-2010 prior to surge initiation. Background image: Rapid-Eye, 06-08-2013; b) WorldView DEM of glacier surface on 17-07-2016, as mass moves from the north arm to the main trunk of Little Kluane Glacier, demonstrating a reverse slope and resulting depression; c) ice elevation profiles of survey line A-A' in 2010 and 2016; d) ice elevation profiles of survey line B-B' in 2010 and 2016. Satellite images courtesy of Planet Labs. The relationship between ice elevation and supraglacial lake location is only shown for the west lake, as DEM coverage does not extend to the east lake.

https://doi.org/10.1017/jog.2024.35 Published online by Cambridge University Press

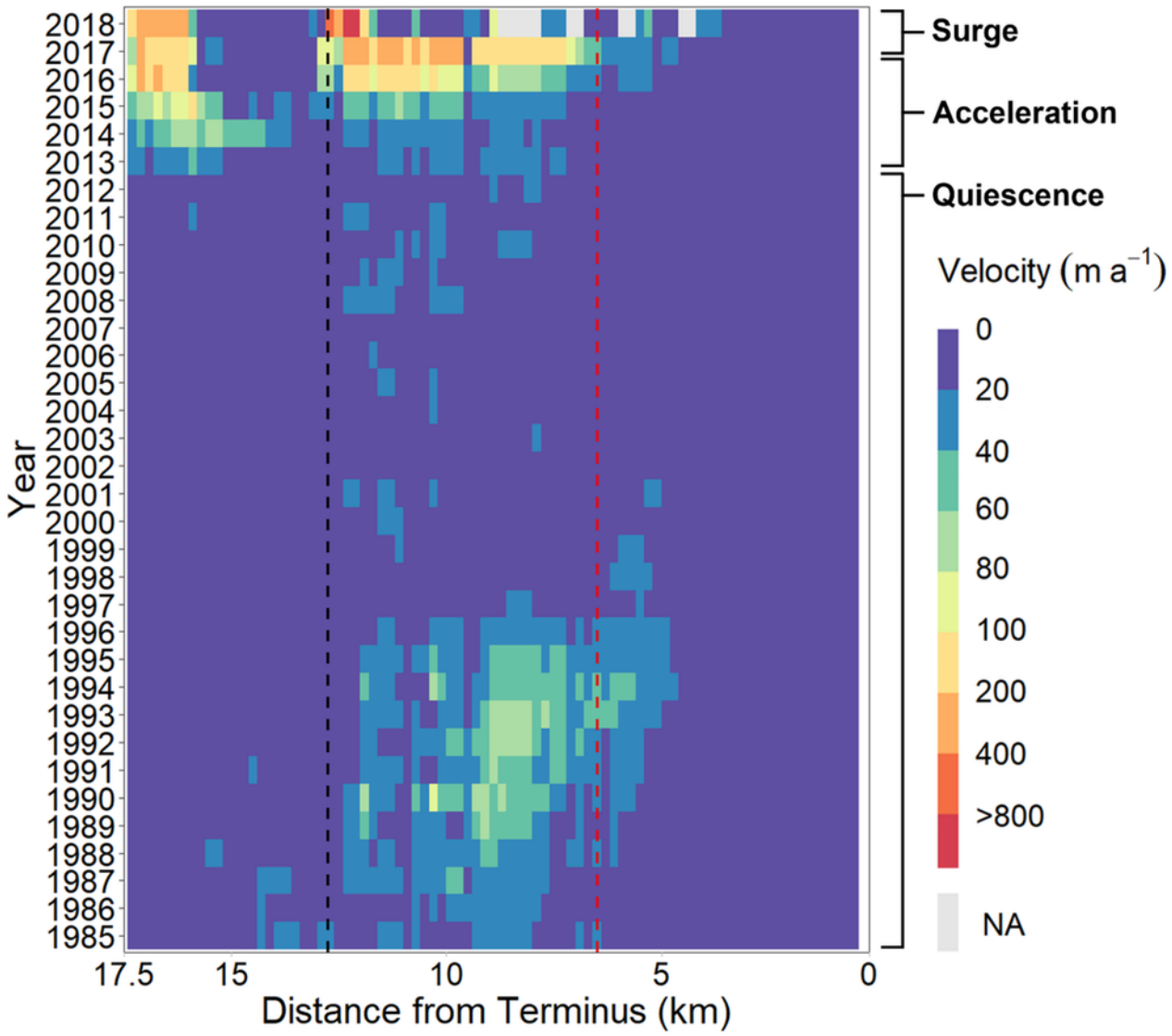

Figure 7: ITS_LIVE velocities along the north arm centreline of Little Kluane Glacier from 1985 to 2018 (see Fig. 1 for location). Dashed black lines indicate where the north arm joins the main glacier trunk. Dashed red line indicates location of the Dynamic Balance Line (DBL), which signifies the transition between the reservoir and receiving zones.

https://doi.org/10.1017/jog.2024.35 Published online by Cambridge University Press

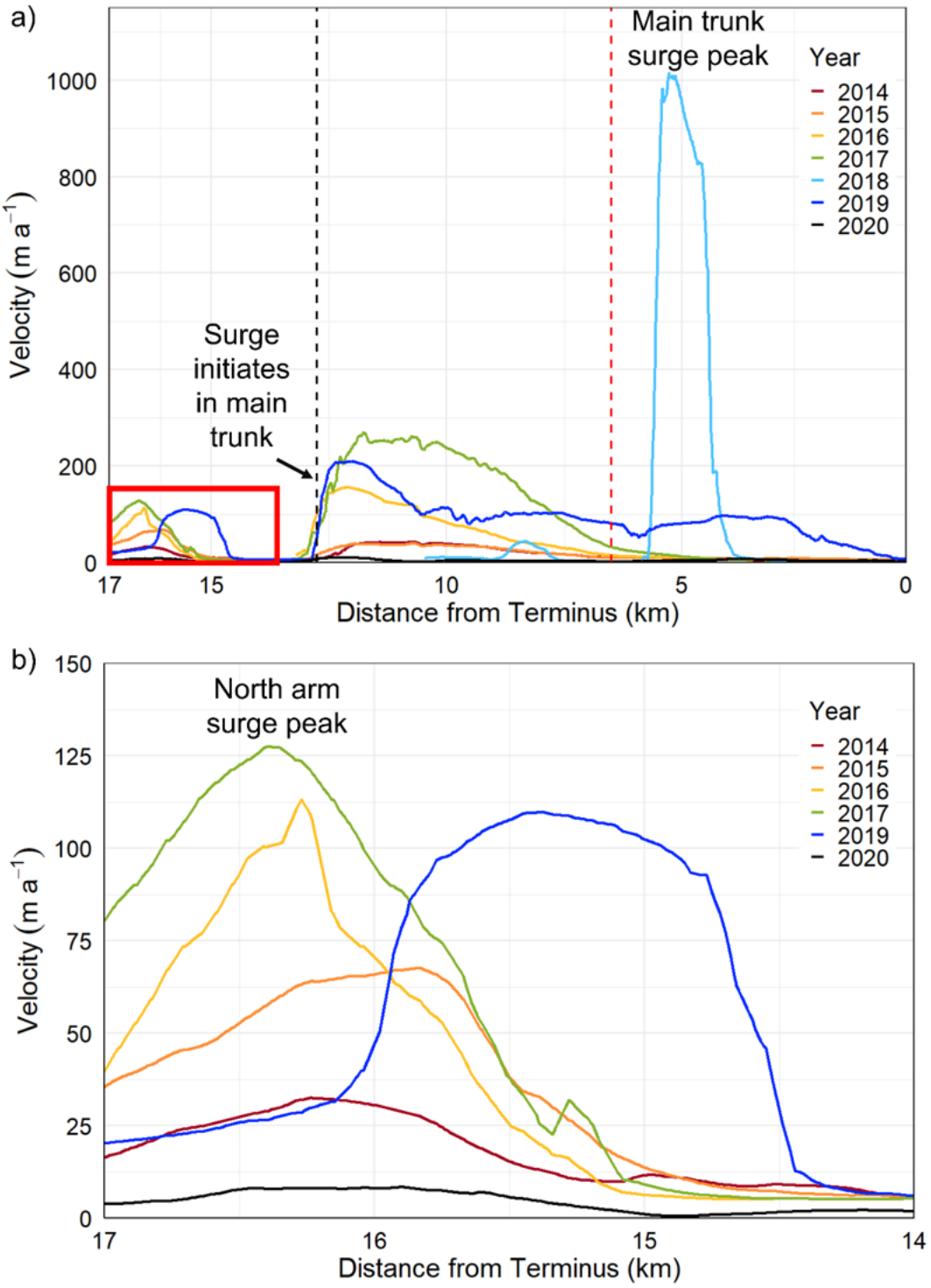

Figure 8: a) Winter (January-May) velocities from RADARSAT-2 data along the north arm centreline of Little Kluane Glacier, 2014-2020. Red box indicates location of zoomed in section in part b). Dashed black lines indicate where the north arm joins the main glacier trunk. Dashed red line indicates the location of the Dynamic Balance Line (DBL); b) Zoom-in to show velocity details for the north arm of Little Kluane Glacier from 2014-2019. Note: there is no data from 2018.

https://doi.org/10.1017/jog.2024.35 Published online by Cambridge University Press